BL-9C, BL-12C/2019G655 and 2019G089

The lowest temperature H_2 reduction of subnano copper oxide particles monitored by *in situ* XAFS measurements

Kazutaka SONOBE,[1] Makoto TANABE,*[2] Takane IMAOKA,*[1,2] Wang-Jae CHUN[3] and Kimihisa YAMAMOTO*[1,2]

[1]Laboratory for Chemistry and Life Science, Tokyo Institute of Technology, Yokohama 226-8503, Japan

[2]JST–ERATO, Yamamoto Atom Hybrid Project, Tokyo Institute of Technology, Yokohama 226-8503, Japan.

[3]Graduate School of Arts and Sciences, International Christian University, Tokyo 181-8585, Japan

Subnanoparticles (SNPs) with sizes of approximately 1 nm are attractive for enhancing the catalytic performance of transition metals and their oxides. Such SNPs are of particular interest as redox-active catalysts in selective oxidation reactions. However, the electronic states and oxophilicity of copper oxide SNPs are still a subject of debate in terms of their redox properties during oxidation reactions for hydrocarbons. In this work, *in situ* X-ray absorption fine structure (XAFS) measurements of $Cu_{28}O_x$ SNPs, which were prepared by using a dendritic phenylazomethine template, during temperature-programmed reduction (TPR) with H_2 achieved lowering of the temperature (T_{50} = 138 °C) reported thus far for the Cu(II)→Cu(I) reduction reaction because of Cu−O bond elongation in the ultrasmall copper oxide particles. Size-controlled Cu_nO_x (n = 12, 28, and 60) materials supported on zirconia, provide size-dependent catalytic activity in aerobic oxidation of the CH_3 group bonded with aromatic rings.

1 Introduction

Oxidation reactions catalyzed by transition-metal oxide nanoparticles (NPs) have recently evolved as a major research area as a result of ongoing efforts to miniaturize processes at the nanoscale.[1] Further miniaturization of oxidized materials to the subnanometer scale (~1 nm) resulting in materials known as metal oxide subnanoparticles (SNPs) has emerged as a novel research concept involving molecular-like chemical properties derived from the discrete electronic levels (quantum size effect) and the amorphous surface geometry of SNPs, which differ completely from those of the corresponding metal oxide crystalline NPs.[2] These unique properties of metal oxide SNPs are expected to lower the high activation barrier in catalytic hydrocarbon oxidation reactions, leading to, for example, the generation of reactive oxygen radicals (O*) suitable for hydrogen abstraction and transfer of the activated oxygen to organic substrates, accompanied by M–O bond scission. Current research interest in such catalytic oxidations is focused on substituting the precious metals with Earth-abundant base metals.

Cu NPs are a particularly important material in catalysis because of the multiple range of accessible oxidation states (Cu(0), Cu(I), and Cu(II)) through one- or two-electron process, which has led to its applications in oxidation/reduction catalysts with unique activity and selectivity. Temperature-programmed reduction (TPR) experiments with CuO NPs in a H_2 atmosphere have revealed that CuO NPs exhibit the lowest reduction temperature among 3*d* transition-metal oxide NPs (i.e., Co_3O_4, NiO, Mn_2O_3, and Fe_2O_3 NPs).[3] This is attributable to Cu−O bonds exhibiting a lower dissociation energy than Co−O, Ni−O, Mn−O, and Fe−O bonds.[4] However, fundamental understanding of the chemical reactivity of copper oxide SNPs is limited and is still a subject of debate.

X-ray absorption fine structure (XAFS) techniques provide atom-specific information about the localized electronic states of Cu and enable predictions of atomic-level structures around Cu. This information is useful in the design of desirable oxidation catalysts and in the proposal of the reaction mechanism. In addition, *in situ* XAFS studies conducted during H_2-TPR experiments provide real-time information related to the variable Cu oxidation states, which are caused by activation of molecular O_2, the release of atomic oxygen on Cu, and intermediate species, depending on the reaction conditions. Rodriguez and coworkers have reported that the reduction of bulk CuO by H_2 [5] via a direct transformation pathway of CuO→Cu proceeds more easily than the reduction of Cu_2O. Similar monitored reductions of CuO NPs (>5 nm) have indicated a sequence pathway (CuO→Cu_2O→Cu) involving a catalytically active Cu(I) intermediate phase.[6] However, the factors governing the formation of the intermediate phase and the effect of smaller particle sizes on these factors are not fully understood.

Therefore, the ability to prepare copper oxide SNPs with a particle size of ~1 nm would be one of the attractive strategies in the design of highly reactive catalysts for hydrocarbon oxidation. Dendrimer-templated preparation is the most effective synthesis strategies for the preparation of size-controlled NPs with a narrow size polydispersity. Fourth-generation dendritic poly(phenylazomethine)s with a tetraphenylmethane core (DPA, Figure 1) have been investigated as templates for preparing SNPs with atomic-level precision.[7] The atom-

specific noble metal SNPs have been reported to show high catalytic performance in electrochemical reactions[8] and in hydrocarbon oxidation using O_2 molecules.[9] Non-noble-metal oxide SNPs exhibit enhanced catalytic performance because of the activation of metal–oxygen bonds or the formation of structural defects on their surface as the size of the SNPs is reduced.[10] In the present study, copper oxide SNPs during TPR experiments with H_2 were monitored by *in situ* XAFS and H_2 consumption measurements. We observed a substantial lowering of the temperature associated with Cu(II)→Cu(I) reduction of the copper oxide SNPs when their particle size was reduced to the subnano order [11].

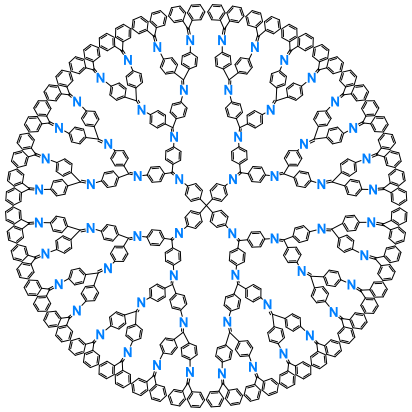

Figure 1. Molecular structure of a fourth-generation (G4) phenylazomethine dendrimer with a tetraphenylmethane core (DPA).

2 Experiment

Chemicals. The $Cu_{28}O_x$@DPA using a fourth–generation phenylazomethine dendrimer with a tetraphenylmethane (DPA) core was synthesized according to the previously reported method.[12] $CuCl_2$ powder (99%, Aldrich), CuO powder (< 50 nm, Aldrich), $Cu(OH)_2$ (Wako), and $NaBEt_3H$ (1.0 M in toluene, Aldrich) were purchased and used as-received. Dehydrated solvents such as toluene, *n*–hexane, $CHCl_3$, and CH_3CN were purchased from Kanto Chemical and used without any purification. The mesoporous silica (MPS, pore size: 7 nm) was received from Aldrich and used after dried *in vacuo* overnight at 200 °C.

XAFS measurements. XAFS was measured in transmission mode at the BL9C beamlines at the High Energy Accelerator Research Organization Institute of Materials Structure Science Photon Factory (KEK-IMSS-PF), Japan. The synchrotron radiation from the storage ring was monochromatized with Si(111) channel-cut crystals, which reduces higher-order harmonics. The angle of the monochromator was calibrated using Cu foil. The ionization chambers, as detectors to monitor the incident (I_0) and transmitted X-rays (I), were filled with N_2 and 50%Ar–50%N_2 mixed gas for the Cu K-edge XAFS, respectively. All samples of the CuO/MPS powder were molded as a pellet with an external diameter of 7 mm. The samples were then loaded into a custom-designed and heat resistant cell and exposed to a flow of a H_2/He mixture gas (20 vol.%/80 vol.%) with a flow rate of 100 cm^3 min^{-1} (Figure 2). The programming rate of 3 °C min^{-1} in the temperature range of 30 °C to 350 °C or 370 °C was set and the Quick-scanning XAFS (QXAFS) scans were taken repeatedly by 180 seconds per scan on heating the sample. The XAFS curve fitting results were obtained by using REX2000 package (Rigaku Co., Japan). The theoretical phase shifts and the amplitude functions for Cu–O used in the fitting routine were calculated on the basis of the FEFF 8.4 theoretical models.

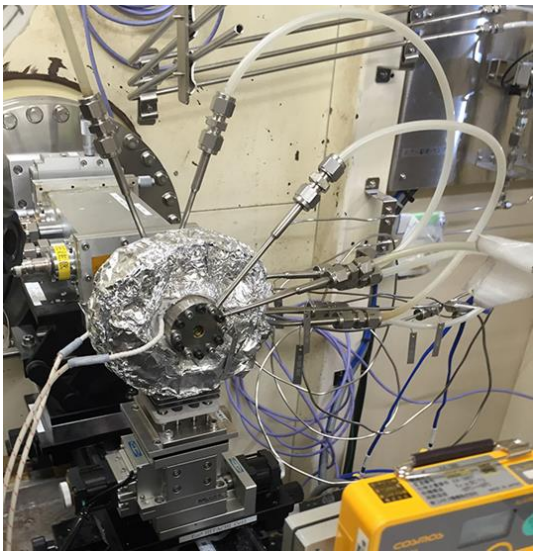

Figure 2. Photograph of a custom-designed and heat resistant cell in the BL 9C beamline.

Temperature programmed reaction measurements. Temperature-programmed reaction (H_2-TPR) measurements were performed using a catalyst analyser (MicrotracBEL, BELCAT II). The copper oxide samples (2 wt%, 100 mg) were loaded into the quarts tube, and then, the measurements were carried out by using H_2/Ar mixture gas (10 vol.%/90 vol.%) with a flow rate of 10 cm^3 min^{-1} and programming rate of 3 °C min^{-1} in the temperature range of 30 to 400 °C. The consumption of H_2 was monitored by thermal conductivity detector (TCD) based on the following two equations: $2\ CuO + H_2 \rightarrow Cu_2O + H_2O$ and $Cu_2O + H_2 \rightarrow 2\ Cu + H_2O$

3 Results and Discussion

Copper oxide SNPs composed of 28 Cu atoms ($Cu_{28}O_x$) were prepared using a DPA template method, similar to the previously reported method (Scheme 1). An approximately equimolar amount of $CuCl_2$ was accumulated by coordination of $CuCl_2$ to the C=N groups in a dendrimer and reduced with a small amount of $NaBEt_3H$ in solution, followed by exposure of the particles to air under ambient conditions and impregnation of the dendrimer-encapsulated particles into mesoporous silica (MPS) with a large pore size (~7 nm). High-angle annular darkfield scanning transmission electron microscopy (HAADF-STEM) images of representative $Cu_{28}O_x$@DPA/MPS particles show a mean diameter of ~1 nm and a narrow size distribution. For comparison, copper oxide NPs (CuONPs) with a larger particle size of 2–3 nm and a wider distribution were also

prepared without the DPA dendrimer template.

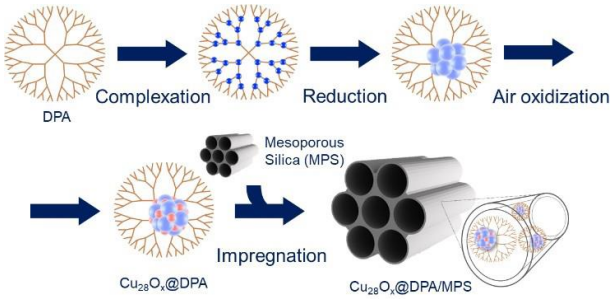

Scheme 1. Schematic preparation of $Cu_{28}O_x$@DPA/MPS.

Figure 3(a) and (b) show Cu K-edge X-ray absorption near-edge structure (XANES) spectra of $Cu_{28}O_x$@DPA/MPS, the prepared CuO^{NPs}/MPS, and a physical mixture of commercially available CuO on MPS (CuO^{COM}/MPS) as a standard reference. The absorption spectra of the $Cu_{28}O_x$ SNPs and CuO^{NPs} are more similar to the spectrum of the $Cu(OH)_2$ than to that of the CuO^{COM}, indicating the presence of OH groups on the surface of the ultrasmall particles. All of the spectra show very small pre-edge peaks at 8975.5 eV. These peaks are associated with the dipole-forbidden 1*s*→3*d* transition, which is ascribed to features typical of the Cu(II) state. The shoulders at 8986.5 eV in the spectra of the $Cu_{28}O_x$ SNPs, CuO^{NPs}/MPS, and $Cu(OH)_2$ correspond to the allowed 1*s*→4*p* transition. Decreasing the particle size to the subnanoscale order led to the emergence of a small edge shoulder at 8983.3 eV, which is similar to the well defined pre-edge feature of the Cu(I) state.[13]

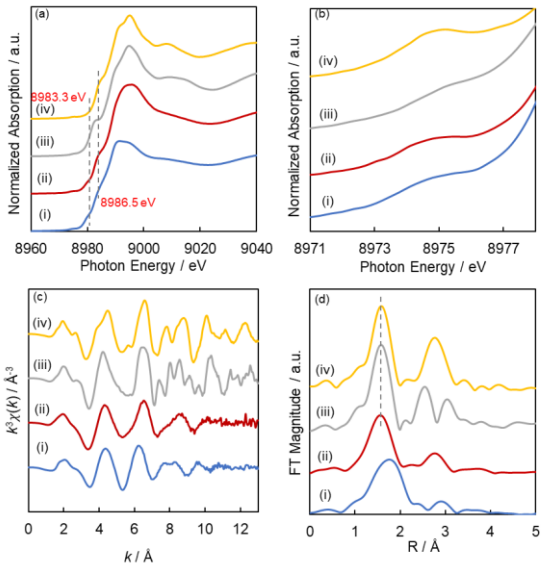

Figure 3. (a) Normalized Cu K-edge XANES spectra, (b) the extend spectra in the pre-edge region, (c) k^3-weighted Cu K-edge $\chi(k)$ EXAFS data and (d) Fourier transform Cu K-edge EXAFS spectra (k^3: $3 \le \Delta k \le 12$ Å^{-1}) of (i) $Cu_{28}O_x$ SNPs (blue), (ii) CuO^{NPs} (red), (iii) CuO^{COM} (gray), and (iv) $Cu(OH)_2$ (yellow).

The Fourier transform of k^3-weighted extended X-ray absorption fine structure (EXAFS) spectra of the $Cu_{28}O_x$ SNPs in the *k*-space range from 3 to 12 Å^{-1}, as shown in Figure 3(d), were also compared with the spectra of CuO^{NPs}, CuO^{COM}, and $Cu(OH)_2$. The large peaks in the first coordination shell ($1.2 \le R \le 2.0$ Å) are attributed to direct Cu–O bonds. The small peaks in the second coordination shell ($2.2 \le R \le 3.0$ Å) are assigned to nonbonding Cu–O–Cu units. Both signals in the spectra of the $Cu_{28}O_x$ SNPs are broadened and shifted toward the elongated bond distances compared with the corresponding peaks in the spectra of the larger CuO^{NPs} and $Cu(OH)_2$ particles. The decrease in magnitude for the second shell of the $Cu_{28}O_x$ SNPs is attributed to their ultrasmall particle size. The curve-fitting results summarized in Table 1 suggest that the Cu–O bond length in the $Cu_{28}O_x$ SNPs is 2.05±0.02 A, which is longer than the Cu–O bond lengths in CuO^{COM} and CuO^{NPs} (1.94 and 1.95 A, respectively). The coordination number for the Cu–Cu bonds in $Cu_{28}O_x$ SNPs was not clearly determined because of the low intensity of the corresponding peaks, whereas that for the Cu–O bonds in $Cu_{28}O_x$ SNPs (3.6±0.6) was greater than those for Cu–O bonds in CuO^{NPs} (2.8±1.7) and CuO^{COM} (2.0±1.0). The XAFS analysis led to the conclusion that the amorphous $Cu_{28}O_x$ SNPs, unlike the crystalline CuO^{NPs}, were covered with OH or H_2O groups on their strained surfaces. The OH group of $Cu_{28}O_x$ SNPs is possible to interact with the surface of the MPS materials rather than encapsulation of the macromolecular ligand, but the detailed structures are not clear.

Table 1 EXAFS analysis data of CuO^{COM}, CuO^{NPs}, and $Cu_{28}O_x$ SNPs[a)]

Sample		N[b)]	r [Å][c)]	ΔE_0 [eV][d)]	σ^2/ 10^{-3} [Å][e)]	R_f [%][f)]
CuO^{COM}	Cu–O	2.5±0.4	1.95±0.01	-5.40±2.96	0.021±0.001	0.79
	Cu–Cu	2.0±1.0	2.85±0.03	-14.41±5.34	0.009±0.002	
CuO^{NPs}	Cu–O	2.7±0.4	1.94±0.01	-4.86±2.55	0.003±0.001	2.73
	Cu–Cu	2.8±1.7	3.04±0.04	6.61±5.41	0.013±0.002	
$Cu_{28}O_x$	Cu–O	3.6±0.6	2.05±0.02	2.07±2.04	0.011±0.001	6.80

[a)] Fourier transform and Fourier filtering regions for all the samples were limited to $\Delta k = 3.0$~12 Å^{-1}, [b)] *N*, coordination number, [c)] *r*, bond distance between absorber and backscatter atoms, [d)] ΔE_0, inner potential correction accounting for the difference in the inner potential between the sample and the reference, [e)] σ^2, the Debye-Waller factor (DW), [f)] R_f (*R*-factor), goodness of curve fitting.

Figures 4(a) and 4(b) show *in situ* Cu K-edge XAFS spectra of CuO^{COM} and $Cu_{28}O_x$ SNPs during the TPR process with H_2. The Fourier transform EXAFS spectra of all samples (k^3: $3 \le \Delta k \le 12$ Å^{-1}) show an increase in the intensity of the metallic Cu–Cu peak (1.5–3.0 A) and a decrease in the intensity of the Cu–O peak (1.0–2.0 A) with increasing temperature. More quantitative results related to the dynamic behavior in the *in situ* XAFS spectra were obtained by linear combination fitting analysis (LCF). The CuO^{COM} solid was directly reduced to metallic Cu(0) without forming Cu_2O or Cu_4O_3 intermediate phases (Figure 4(c)), similar to previously reported results,[5] because the reduction of CuO is easier than the reduction of thermally stable Cu_2O. The LCF results for CuO^{COM} show a slow conversion at ~230 °C, indicating that reduction proceeds at limited surface sites

or lattice defects in the CuO NPs. The temperature associated with 50% conversion (T_{50}) was estimated to be 293 °C for the direct reduction from Cu(II) to Cu(0). By contrast, the $Cu_{28}O_x$ SNPs and CuO^{NPs} underwent sequential reduction via the formation of a Cu(I) intermediate, as evidenced by the typical peak corresponding to Cu(I) (8980 eV) being observed within a wide temperature range between 75 and 370°C (Figure 4(d)). The LCF for the $Cu_{28}O_x$ SNPs shows a steep slope associated with both the Cu(II)→Cu(I) and Cu(I)→Cu(0) reductions. The lower T_{50} of 138 °C for the first step is attributed to the facile dissociation of atomic oxygen from the elongated Cu–O bonds of the amorphous copper oxides. The second reduction, Cu(I)→Cu(0), occurred at a slightly higher T_{50} (306 °C) compared with that for the direct reduction of CuO^{COM} (T_{50} = 293°C) because of the thermally stable Cu(I) state.

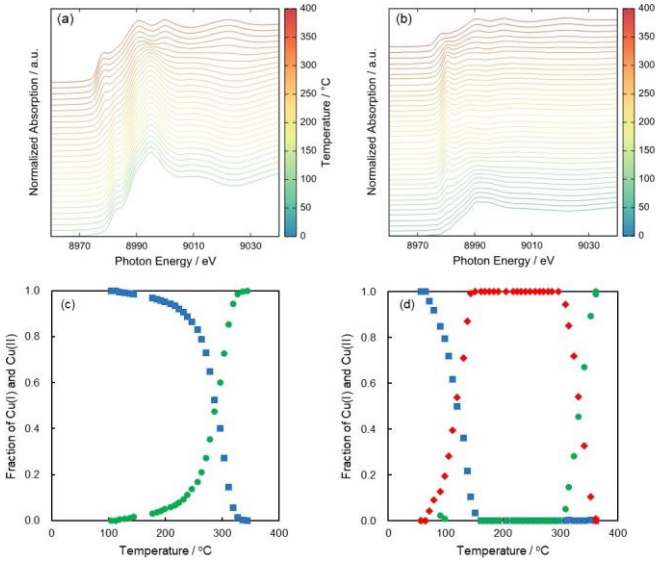

Figure 4. Normalized XANES spectra of (a) CuO^{COM} and (b) $Cu_{28}O_x$ SNPs in the Cu K-edge region during temperature-programmed reduction in 20% H_2/He (H_2-TPR) at a rate of 3 °C/min between 30 and 350 or 370°C. Fraction of Cu(II) (blue), Cu(I) (red), and Cu(0) (green) from the LCF results of Cu K-edge XANES spectra of (c) CuO^{COM} and (d) $Cu_{28}O_x$ SNPs during the H_2-TPR experiments.

Figure 5 shows the H_2-TPR profile for the $Cu_{28}O_x$ SNPs, along with the Cu fractions from the LCF analysis (Figure 4(d)). The profile shows two H_2 consumption peaks with almost the same peak area because an equimolar amount of H_2 was consumed during each reduction. The T_{50} temperatures of 138 and 306 °C, as monitored by *in situ* XAFS measurements, are in the temperature range of H_2 consumption in the Cu(II)→Cu(I) and Cu(I)→Cu(0) reductions. The H_2-TPR of CuO^{COM} exhibited direct Cu(II)→Cu(0) reduction corresponding to T_{50} = 293°C, which is close to the Cu(I)→Cu(0) reduction temperature of the $Cu_{28}O_x$ SNPs. Notably, the copper oxide SNPs exhibited the lowest Cu(II)→Cu(I) reduction temperature than the corresponding NPs and copper oxides supported on zeolites because of their subnanoscale particle size, to the best of our knowledge.

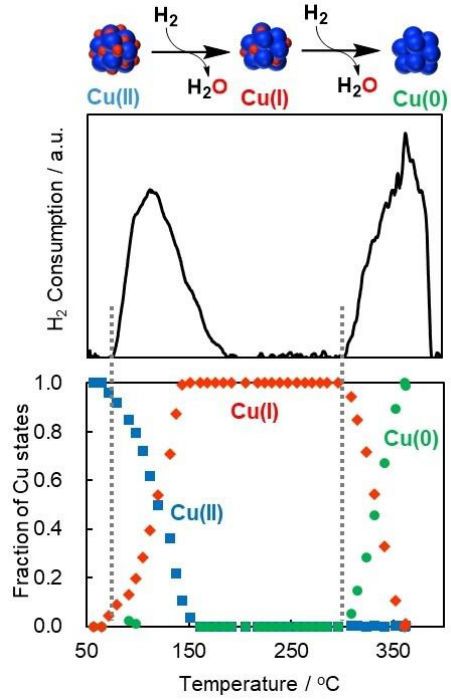

Figure 5. Relationships between H_2 consumption and fraction of Cu oxidation states for $Cu_{28}O_x$ SNPs during the H_2-TPR experiments.

In summary, we have demonstrated the dynamics of the size-dependent H_2 reduction of CuO particles with sizes ranging from large NPs (~50 nm) to ultrasmall SNPs (~1 nm), which were monitored by *in situ* XAFS measurements. Interestingly, the CuO SNPs exhibited the lowest Cu(II)→Cu(I) reduction temperature directly observed by *in situ* XAFS measurements; the temperature for further reduction of Cu(I) to metallic Cu(0) was found to be independent of the particle size. The CuO particles with low atomicity easily release oxygen atoms because of their surface-strained structure and the unprecedented elongation of their Cu−O bonds. This work provides a strategy for preparing catalytically enhanced Cu_nO_x SNPs (n = 12, 28, 60) on ZrO_2 for aerobic toluene oxidation reactions under ambient temperature.[12]

Acknowledgement

The acknowledgement section is optional. If you do not need it, please delete this section. We thank the PF staff for creating this template. This study was supported by an ERATO Grant (No. JPMJER1503 (K.Y.)) and an A-STEP (No. JPMJTM20DB (M.T.)) from the Japan Science, Technology Agency (JST) and a Kakenhi Grant-in-Aid for Scientific Research (S) (No. 15H05757 (K.Y.)). This work was performed under the Cooperative Research Program of "Network Joint Research Center for Materials and Devices (W.-J.C.)". XAFS measurements were conducted at the BL-9C beamlines of the High Energy Accelerator Research Organization-Institute of Materials Structure Science-Photon Factory (KEK-IMSS-PF) under the approval of the Photon Factory Advisory (Proposal numbers 2019G655 and 2019G089).

References

[1] I. Hermans, *et al.*, *Chem. Rev.* **118**, 2769 (2018).
[2] D. Astruc, *et al.*, *Chem. Rev.* **120**, 526 (2020).
[3] A. A. Khodadadi, *et al.*, *Appl. Catal. A Gen.* **477**, 159 (2014).
[4] Y. Shiota and K. Yoshizawa, *J. Am. Chem. Soc.* **122**, 12317 (2000).
[5] J. A. Rodriguez, *et al.*, *J. Am. Chem. Soc.* **125**, 10684 (2003).
[6] a) J. D. Grunwaldt, *et al.*, *J. Phys. Conf. Ser.* **2009**, **190**, 012153 (2009); b) J. A. Rodriguez, *et al.*, *J. Phys. Chem. B* **108**, 13667 (2004); c) J. Hanson, *et al.*, *Appl. Catal. A. Gen.* **303**, 273 (2006).
[7] a) K. Yamamoto, *et al.*, *Nature* **415**, 509 (2002); b) K. Yamamoto and T. Imaoka, *Acc. Chem. Res.* **47**, 1127 (2014); c) K. Yamamoto, T. Imaoka, M. Tanabe and T. Kambe, *Chem. Rev.* **120**, 1397 (2020); d) T. Tsukamoto, T. Kambe, T. Imaoka and K. Yamamoto, *Nat. Rev. Chem.* **5**, 338 (2021).
[8] a) K. Yamamoto, T. Imaoka, W.-J. Chun, *et al.*, *Nat. Chem.* **1**, 397 (2009); b) T. Imaoka, H. Kitazawa, W.-J. Chun, K. Albrecht, K. Yamamoto, *et al.*, *J. Am. Chem. Soc.* **135**, 13089 (2013); c) T. Imaoka, H. Kitazawa, W.-J. Chun, K. Yamamoto, *et al.*, *Angew. Chem., Int. Ed.* **54**, 9810 (2015).
[9] a) M. Takahashi, W.-J. Chun, T. Imaoka, K. Yamamoto, *et al.*, *Sci. Adv.* **3**, e1700101 (2017); b) M. Huda, M. Tanabe, K. Yamamoto, *et al.*, *Angew. Chem., Int. Ed.* **58**, 1002 (2019); c) T. Tsukamoto, M. Tanabe, T. Kambe, K. Yamamoto, *et al.*, *Angew. Chem., Int. Ed.* **59**, 23051 (2020).
[10] a) K. Yamamoto, *et al.*, *Nat. Nanotech.* **3**, 106 (2008); b) K. Albrecht, K. Yamamoto, *et al.*, *ACS Catal.* **8**, 451 (2018); c) A. Kuzume, N. Haruta, K. Yamamoto *et al.*, *Sci. Adv.*, **5**, eaax6455 (2019).
[11] K. Sonobe, M. Tanabe, T. Imaoka, W.-J. Chun and K. Yamamoto, *Chem. Eur. J.*, **27**, 8452 (2021).
[12] K. Sonobe, M. Tanabe and K. Yamamoto, *ACS Nano*, **14**, 1804 (2020).
[13] J. A. van Bokhoven, *et al.*, *Chem. Rev.*, **113**, 1736 (2013).

*tanabe.m.aa@m.titech.ac.jp,
timaoka@res.titech.ac.jp,
yamamoto@res.titech.ac.jp